Wave propagation in coupled periodic lattices and application to vibration attenuation through a piezoelectric network

B. Lossouarn [1], **J.-F. Deü** [1], **M. Aucejo** [1]
[1] Conservatoire National des Arts et Métiers, Structural Mechanics and Coupled Systems Laboratory, 2 rue Conté, 75003, Paris, France
e-mail: **boris.lossouarn@cnam.fr**

Abstract
As described by Brillouin from the 1940's, elastic lattices of point masses can be a suitable representation of continuous structures for the study of wave propagation. By extrapolating the tuned mass damping strategy to lattices of point masses, a multimodal effect is obtained by coupling two structures presenting the same modal characteristics. Consequently, it is theoretically possible to damp vibrations of a mechanical medium thanks to a connection to its discrete electrical equivalent. The coupling between the two structures can be conducted by distributing periodically piezoelectric elements that are linked together with the electrical network. Compared to the more classical independent resonant shunts, this solution stands out from its broadband capabilities and the possibility to design a completely passive system. This concept is numerically and experimentally validated through the study of wave propagation in one-dimensional electromechanical structures.

1 Introduction

Over the last few years, periodic structures received much attention because of their interesting property to present stop bands that attenuate wave propagation on particular frequency ranges. In this context, homogeneous or nearly homogeneous structures can be classified as periodic structures but without offering any significant stop band effect. Nevertheless, the methods developed for periodic structures can apply to this particular case.

One of the most popular way to study wave propagation in one dimensional periodic structures is the transfer matrix formalism [1]. This approach is based on the concept of a unit cell, which periodically repeats by keeping the same mechanical properties. Thus, both mechanical states at the ends of a cell respect a relation represented by a constant transfer matrix. This relation is then propagated to obtain the global behavior of a finite structure. The method can apply together with a finite element formulation as it is seen in the Wave Finite Element Method [2]. This allows one to considerably decrease the size of a periodic problem by focusing only on the mesh of a single unit cell. For the analysis of longitudinal waves, the use of only one element per unit cell is after all quite close to the discretization into lattice of point masses as studied by Brillouin in 1946 [3]. He presented several fundamental results related to wave propagation in mechanical as well as electrical periodic structures. An electromechanical analogy was thus already introduced between lattices of different nature, which was then formalized by Beranek for more general structures [4].

The electromechanical analogy can apply to the study of coupled problems focusing on vibration damping by shunted piezoelectric patches [5]. It is seen that the use of resonant shunts is equivalent to the addition of a tuned mass damper [6]. Consequently, by tuning the electrical components, important vibration reduction of a structure can be expected [7]. This concept was applied by Thorp et al. for the damping of longitudinal

waves in a rod periodically covered with piezoelectric patches [8]. The use of the transfer matrix formulation allows studying the propagation constants as well as the global behavior of a finite structure. It was then extended to the study of transverse waves by taking into account the influence of various shunts either passive as the resonant ones [9] or active as those presenting negative capacitors [10]. However, just a few studies consider electrical connections otherwise than independently between the different piezoelectric patches. One can mention Yu et al. [11] who analyze the use of an electric network in order to delocalize vibration in a periodic blade assembly. Closer to real damping of vibration, Maurini et al. [12] present the effects of various networks on transverse wave propagation. From a continuous formulation, one optimal architecture appears to be the electric analogue of a beam [13]. None of the aforementioned studies on electrical networks benefits from the transfer matrix method. This was still performed by Lu and Tang who added electrical components into the state vector for the analysis of a particular periodic network [14].

The present work deals with most of the above cited concepts in order to present a multimodal damping strategy for longitudinal waves. First of all, the transfer matrix formulation is presented and applied to the analysis of a continuous rod which is then discretized into a lattice of point masses. Considering a finite lattice, two possibilities based on modal coupling are presented to convert the vibration energy of a main structure into a damping device. An electromechanical analogy along with a global model of a piezoelectric element show that the two coupling strategies correspond to the ones that could be used to damp vibration of a rod periodically fitted with piezoelectric patches. The first strategy is equivalent to the use of independent resonant shunts while the second leads to the implementation of a real electrical network that presents multimodal properties. Here, the modeling of a continuous mechanical structure into a discrete lattice offers new analysis alternatives, as the electromechanical analogy, that leads to a simplified global model at the level of the coupled unit cells. All of this is validated experimentally by using only standard passive components. Finally, an extension to transverse wave is performed and this shows promising results on multimodal damping.

2 Wave propagation in one-dimensional periodic structures

2.1 Transfert matrix formulation

As presented by Mead, a one-dimensional periodic structure can be described as a succession of identical unit cells [1]. Having the same properties, each one presents the same relation between the mechanical states at its right and left ends. This relation can be described by a transfer matrix $\boldsymbol{T}$ involved in the following equation:

$$\begin{pmatrix} \boldsymbol{q_R} \\ \boldsymbol{F_R} \end{pmatrix} = \boldsymbol{T} \begin{pmatrix} \boldsymbol{q_L} \\ \boldsymbol{F_L} \end{pmatrix}, \tag{1}$$

where $\boldsymbol{q}$ and $\boldsymbol{F}$, constituting the state vectors, refer to the displacements and forces at positions defined by the subscripts $\boldsymbol{L}$ or $\boldsymbol{R}$ for the left or right ends of the unit cell. $\boldsymbol{F_R}$ is the force applied on the considered cell by its right neighbor and $\boldsymbol{F_L}$ is the force applied by the considered cell on its left neighbor. This convention allows keeping the continuity of the state vector which is obvious for the displacements but not systematic for the forces.

Considering a same transfer matrix for each unit cell and a continuity of the state vector, the relation between the states at the ends of a finite periodic structure consisting of N unit cells is obtained by raising $\boldsymbol{T}$ to the power of N. Since the structures are considered as finite, the solution of the problem requires to consider the boundary conditions. For example, with a prescribed force $\boldsymbol{F_0}$ applied to the left end of a free-free structure, the displacement $\boldsymbol{q_N}$ at the right end is defined by:

$$\boldsymbol{q_N} = (\boldsymbol{T_{qF}} - \boldsymbol{T_{qq}}\boldsymbol{T_{Fq}}^{-1}\boldsymbol{T_{FF}})\boldsymbol{F_0}, \quad \text{if} \quad \boldsymbol{T^N} = \begin{pmatrix} \boldsymbol{T_{qq}} & \boldsymbol{T_{qF}} \\ \boldsymbol{T_{Fq}} & \boldsymbol{T_{FF}} \end{pmatrix}. \tag{2}$$

2.2 Longitudinal propagation in a continuous rod

A continuous rod with constant section and constant material properties can be seen as a particular periodic structure in which the number of unit cells remains free. The local behavior is the same all along the structure and each unit cell of length a can be studied as an independent rod. A space-time separation of the wave equation leads to the dispersion relation and the solution for the longitudinal displacement $U(x)$:

$$\omega^2 = \frac{Y}{\rho}k^2 \quad \text{and} \quad U(x) = U_L\cos(kx) + \frac{U_R - U_L\cos(ka)}{\sin(ka)}\sin(kx), \tag{3}$$

where Y and ρ are respectively the Young modulus and the density of the rod. The ratio of those constants defines the square of the phase velocity that links the circular frequency ω to the wavenumber k. Regarding the boundary conditions, they appear directly into the equation for the displacement as the subscripts L and R refer to the position $x = 0$ and $x = a$.

Then, the normal force into the rod being proportional to the first derivative of the displacement presented in Eq. (3), i.e. $N(x) = YSU'(x)$, the end forces are linearly related to the end displacements, which can be rearranged into the following matrix form:

$$\begin{pmatrix} U_R \\ N_R \end{pmatrix} = \begin{pmatrix} \cos(ka) & \dfrac{1}{YSk}\sin(ka) \\ -YSk\sin(ka) & \cos(ka) \end{pmatrix} \begin{pmatrix} U_L \\ N_L \end{pmatrix}, \tag{4}$$

where S is the rod section. This corresponds to the transfer matrix formulation described in Eq. (1), the state vector containing in this case the longitudinal displacement U and the normal force N. At the end, considering a free-free rod of length $l = Na$ excited at one end, it is possible from Eq. (2) to get the frequency response of the displacement at the other end.

2.3 Discrete model for the longitudinal waves

The purpose of the previous formulation is not obvious for a strictly continuous structure as the global solution can be directly obtained from the analysis of a single unit cell of length l (with $N = 1$). Nevertheless, the transfer matrix becomes useful when looking at a discretized model where the global layout is not identical to the local one. Concerning the study of the propagation of longitudinal waves, Brillouin studied the discretization of a continuous medium by the use of a lattice of point masses [3]. This can apply to a rod by considering periodically lumped masses m linked together by springs of identical stiffness K. The unit cell can thus be defined by two half masses at each ends of a spring as presented in Figure 1.

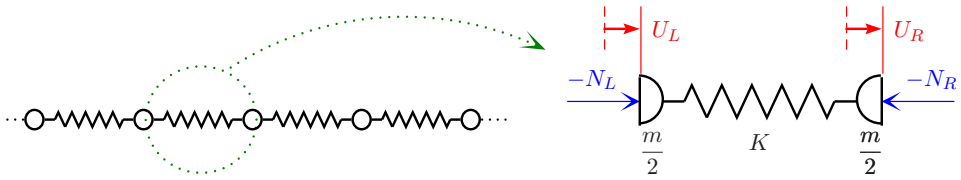

Figure 1: Unit cell of a discretized rod

Consequently, the mass and the stiffness are determined from the local properties of the rod and the length a of the unit cell:

$$m = \rho Sa \quad \text{and} \quad K = \frac{YS}{a}. \tag{5}$$

It is manifest that the length of the cell needs to be consequently smaller than the wavelength to be analyzed. In a classical manner as for some Wave Finite Element studies, a limit can be fixed to 10 elements per wavelength [2]. The dispersion relation presented in Eq. (3) leads to a frequency limit, which is equivalent

to restrict the analysis to the most linear part of the lattice dispersion curve [3]. This limits phenomenon due to the discretization and thus approximates a continuous behavior.

Performing the mechanical analysis of the unit cell gives the relation between both state vectors containing the displacement and the normal force at each end. This corresponds to the transfer matrix formulation of the discretized rod:

$$\begin{pmatrix} U_R \\ N_R \end{pmatrix} = \begin{pmatrix} 1-f & \frac{1}{K} \\ -2Kf\left(1-\frac{f}{2}\right) & 1-f \end{pmatrix} \begin{pmatrix} U_L \\ N_L \end{pmatrix}, \quad \text{where} \quad f = \omega^2 \frac{m}{2K}. \tag{6}$$

One can remark that for both transfer matrix presented in Eqs. (4) and (6), the approximation to their 2nd degree Taylor polynomial in a are equal. This confirms that the presented discrete model tends to the continuous one when the length of the unit cell is sufficiently small compared to the considered wavelength.

3 Energy conversion based on modal coupling

3.1 Distributed tuned mass dampers

In order to control the vibration of a finite periodic structure, a possibility is to add multiple damping devices locally, at the level of the unit cell. When looking at passive solutions, the tuned mass damping strategy is suitable to convert energy from a main structure to the added mass at one particular frequency, which is chosen by tuning the resonance of the added system. This can apply to the lattice by distributing identical tuned mass systems to each of the unit cells, as in the Vincent's model [3]. In a close way, a solution is presented in Figure 2, where a strain in the main structure is converted into a displacement of the added system thanks to a lever of e ratio. This stresses the spring of stiffness $\hat{K}$ and thus put the tuned mass $\hat{m}/4$ in motion.

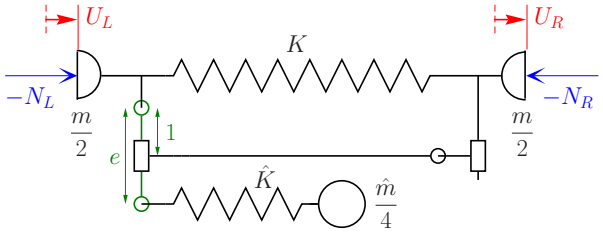

Figure 2: A tuned mass damper fixed to each unit cell

As achieved previously for the basic unit cell, the mechanical analysis of this new sub-structure can be realized for the purpose of getting the transfer formulation of the problem. For small displacements and a small mass $\hat{m}/4$ compared to m, the following matrix is obtained:

$$\begin{pmatrix} U_R \\ N_R \end{pmatrix} = \begin{pmatrix} 1-f\tilde{f} & \frac{\tilde{f}}{K} \\ -2Kf\left(1-\frac{f\tilde{f}}{2}\right) & 1-f\tilde{f} \end{pmatrix} \begin{pmatrix} U_L \\ N_L \end{pmatrix}, \quad \text{where} \quad \tilde{f} = \frac{1-\omega^2\frac{\hat{m}}{4\hat{K}}}{1-\omega^2\frac{\hat{m}}{4}\left(\frac{e^2}{K}+\frac{1}{\hat{K}}\right)}, \tag{7}$$

which shows that for $\omega = \sqrt{4\hat{K}/\hat{m}}$, $\tilde{f}$ becomes equal to zero. Therefore, at the natural frequency of the added spring mass system, the displacement is the same in all the primary lattice, no strain is observable whatever the boundary conditions. The effect of the distributed tuned mass dampers on a finite structure can be illustrated through the example of a $l = 1$ m free-free duralumin rod discretized in $N = 20$ unit cells,

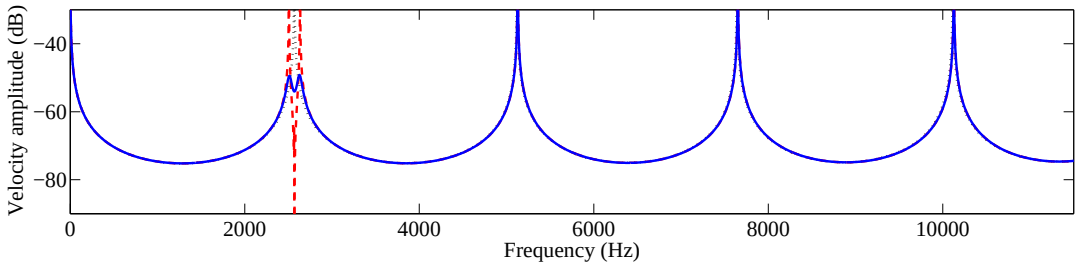

Figure 3: Distributed tuned mass dampers - $(\cdots)$ for $e = 0$, $(--)$ for $e = 1$, $c = 0$ and $(—)$ for $e = 1$, $c = 1$

each one being fitted with identical tuned mass dampers. The cross-section of the rod is taken equal to $S = 4$ cm^2, its Young modulus is $Y = 74$ GPa and its density $\rho = 2800$ kg/m^3. The added mass $\hat{m}/4$ is then set to one tenth of the mass m and $\hat{K}$ is tuned so that the natural frequency of the spring-mass system corresponds to the first natural frequency of the continuous rod. One can remark that there is necessarily a difference between the natural frequencies of the continuous structure and those of its discrete model. Nevertheless, this difference is acceptable if the number of unit cell per wavelength is sufficiently high. In our example, the aforesaid limit of 10 elements per wavelength induces a maximum frequency at the 4^{th} mode of the free-free rod as it is discretized in 20 unit cells. If a study at higher frequency is required, the increase of N is desirable in order to approximate the continuous behavior.

The numerical results are presented in Figure 3 for the end velocity, which is obtained by the combination of Eqs. (2) and (7) followed by a temporal derivative. No damping is introduced into the rod model but the plot of the velocity amplitude is limited to -30 dB at maximum, which suits to experimental observations. When the lever ratio e is equal to 0, the lattice behaves without any effect of the added system. With $e = 1$ and no damping in the tuned mass system, one can remark that around the first natural frequency the initial resonance is no more observable as the energy is transferred to the added mass. Yet, two new resonances appear either sides of the previous one. For the sake of limiting the velocity amplitude all around the initial first natural frequency of the rod, the solution provided in most of the tuned mass damping strategies consists in adding a damper in parallel to the spring of stiffness $\hat{K}$. However, it is also possible to consider a damper linking directly the tuned mass to the ground [6]. This last solution is here implemented by replacing $\hat{m}/4$ by $\hat{m}/4 - jc/\omega$, where c is the damping coefficient. With $c = 1$ N/(m/s), the amplitude is considerably reduced to about -50 dB, which illustrates the efficiency of the strategy.

3.2 Multimodal tuned mass damper

By extrapolating the previous concept that consists in linking two structures that have one common resonance frequency, it would be interesting to couple two multimodal structures presenting a similarity for all their modes. In our case, considering two rods of same length and same boundary conditions, it is possible to show from Eq. (3) that a similar dispersion relation (a same ratio Y/ρ) induces the equality of the natural frequencies. So, for rods discretized with the same length a, this is equivalent to equalize the ratio K/m in the two lattices. Starting from this modal coupling condition, it is then needed to find a way to mechanically connect the two structures in order to allow energy transfers within each pair of unit cells. A solution is presented in Figure 4 as a generalization of the previous tuned mass damper architecture. The fundamental difference is here that the added masses are not free but linked to their own lattice. When considering a lever ratio e equal to 0, the two lattices are completely decoupled, which is equivalent to study two independent structures as the one introduced in Figure 1. On the contrary, if e is different to zero, the two lattices exchange energy through the lever mobility, that exhibits a tuned mass effect on all the resonances if the modal coupling condition is observed together with an equivalence of the boundary conditions. As previously, this can be shown by the analysis of a finite discretized free-free rod coupled with its modal equivalent.

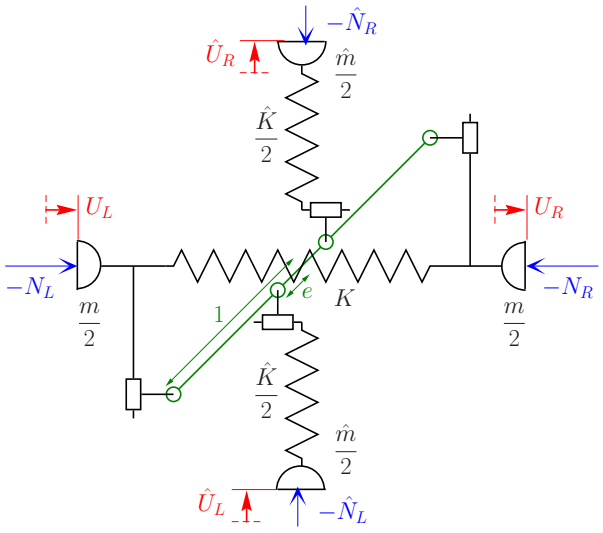

Figure 4: Unit cell for two coupled discretized rods

The global analysis requires firstly the study of the mechanical problem presented in Figure 4, which leads to the following formulation for small displacements:

$$\begin{pmatrix} U_R \\ \hat{U}_R \\ N_R \\ \hat{N}_R \end{pmatrix} = \begin{pmatrix} 1-f_l & e\frac{\hat{K}}{K}\hat{f} & \frac{1}{K} & -\frac{e}{K} \\ ef_l & 1-\hat{f}\left(1+e^2\frac{\hat{K}}{K}\right) & -\frac{e}{K} & \frac{e^2}{K}+\frac{1}{\hat{K}} \\ -2Kf\left(1-\frac{f}{2}\right) & -e\hat{K}f\hat{f} & 1-f & ef \\ -e\hat{K}f\hat{f} & -2\hat{K}\hat{f}\left[1-\frac{\hat{f}}{2}\left(1+e^2\frac{\hat{K}}{K}\right)\right] & e\frac{\hat{K}}{K}\hat{f} & 1-\hat{f}\left(1+e^2\frac{\hat{K}}{K}\right) \end{pmatrix} \begin{pmatrix} U_L \\ \hat{U}_L \\ N_L \\ \hat{N}_L \end{pmatrix}, \tag{8}$$

$$\text{where} \quad f = \omega^2\frac{m}{2K} \quad \text{and} \quad \hat{f} = \omega^2\frac{\hat{m}}{2\hat{K}}.$$

The presented transfer matrix is then used in the computation of the frequency response function of the velocity at the right end of the rod thanks to Eq. (2). Both normal forces at the two ends of the added structure are set to zero in order to satisfy the equivalence of the boundary conditions with the main free-free rod. Next, it is arbitrary chosen to enforce the mass $\hat{m}$ to one hundredth of m and e equal to 1. At last, the modal coupling condition gives the value of $\hat{K} = \hat{m}K/m$ which allows tuning the resonance frequencies of the damping structures to those of the duralumin discretized rod.

The results of the multimodal damping are shown in Figure 5. One can remark that the shape of the curves is the same than for the distributed tuned mass dampers but here the effect is observable for all the natural

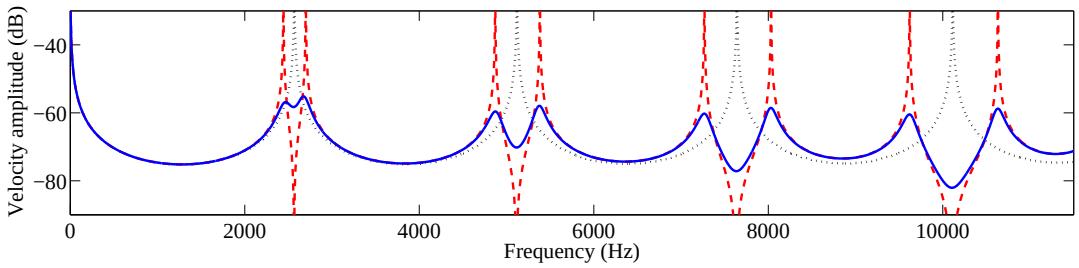

Figure 5: Multimodal damping - $(\cdots)$ for $e = 0$, $(--)$ for $e = 1$, $c = 0$ and $(—)$ for $e = 1$, $c = 1$

frequencies. As previously, addition of damping applying on the displacement of the masses $\hat{m}$ reduces considerably the velocity amplitude. This reduction is pronounced all along the presented frequency range, which highlights the power of the multimodal damping.

4 Damping strategies by the use of piezoelectric elements

4.1 Electrical equivalents

The discretized models presented in Sections 2 and 3 can be transposed to electrical architectures by using the direct electromechanical analogy [4]. This method assumes the equivalence between mass and inductance, stiffness and inverse of a capacitance, force and voltage and velocity and intensity. Thereby, the discretized rod is equivalent to an electrical network made of a line of inductors with connections to the ground through capacitors. This line is illustrated in Figure 6 together with the corresponding electrical unit cell.

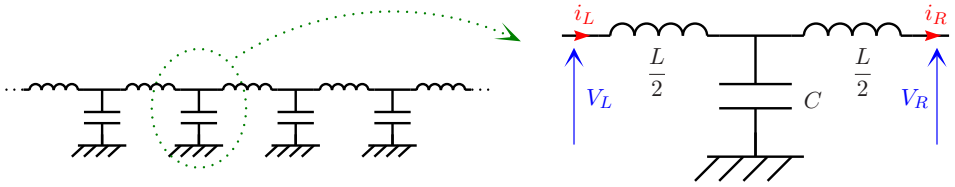

Figure 6: Electrical equivalent of the discretized rod and the corresponding unit cell

The analogues of the left and right intensities are thus the derivatives of the left and right displacements, and in order to respect the definition of the forces, the two voltages are their opposites. The resulting equations are strictly identical to the mechanical ones by taking $m = L$ and $K = 1/C$. Consequently, from Eq. (6), the transfer matrix can be expressed under the form

$$\begin{pmatrix} i_R \\ V_R \end{pmatrix} = \begin{pmatrix} j\omega & 0 \\ 0 & -1 \end{pmatrix} \begin{pmatrix} 1-f & C \\ -\frac{2}{C} f \left(1 - \frac{f}{2}\right) & 1-f \end{pmatrix} \begin{pmatrix} \frac{1}{j\omega} & 0 \\ 0 & -1 \end{pmatrix} \begin{pmatrix} i_L \\ V_L \end{pmatrix}. \tag{9}$$

As for the discretized rod, it is possible to consider the coupling of two electrical networks. Here, it is a transformer that converts the energy from a network to the other. This one has the same role than the lever in the mechanical model and finally the complete analogue of the coupled mechanical unit cell of Figure 4 is presented in Figure 7. Again, with $L = m$, $C = 1/K$, $\hat{L} = \hat{m}$, $\hat{C} = 1/\hat{K}$, $i = j\omega U$ and $V = -N$, the resulting equations are strictly the same than for the mechanical structure and the electric transfer matrix can thus be deduced from Eq. (8). By setting $\hat{V}_L = \hat{V}_R = 0$, the electric scheme of Figure 7 applies also to the more particular case of the electrical analogue of the tuned mass damper, consisting in a capacitor $\hat{C}$ and an inductor $\hat{L}/4$ in parallel. It is equivalent the to mechanical representation developed in Figure 2, and that explains more easily why the added mass was set to $\hat{m}/4$.

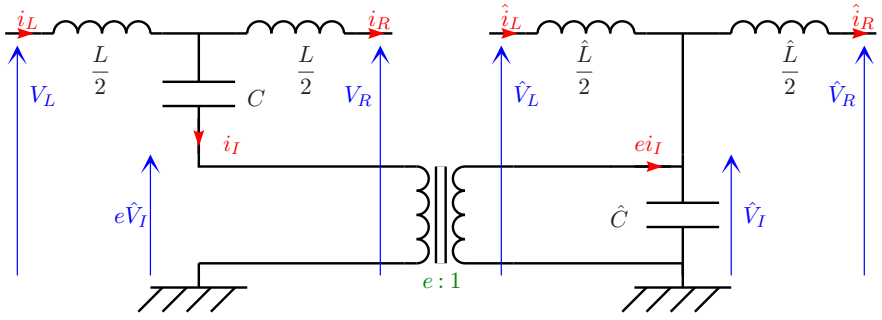

Figure 7: Coupling of two electrical networks

4.2 Model for the piezoelectric elements

The representation of the coupling of two electrical networks designed from an electromechanical analogy guides to the concept of connecting two similar structures of different natures, one mechanical and one electrical. This requires a component capable of converting mechanical energy into electric energy. Piezoelectric material fulfills this function as shown in many studies focusing on passive vibration control [7, 8, 9, 12, 5, 13, 14]. Those ones consider linear piezoelectricity as valid for the considered range of vibration and the 3D formulation can be simplified for rods into the following one-dimensional stress-charge form [7]:

$$\begin{cases} \sigma = \bar{c}_{11}^{E}\varepsilon - \bar{e}_{31}E \\ D = \bar{e}_{31}\varepsilon + \bar{\epsilon}_{33}^{\varepsilon}E \end{cases}, \quad \text{where} \quad \bar{c}_{11}^{E} = \frac{1}{s_{11}^{E}}, \quad \bar{e}_{31} = \frac{d_{31}}{s_{11}^{E}} \quad \text{and} \quad \bar{\epsilon}_{33}^{\varepsilon} = \epsilon_{33}^{\sigma} - \frac{d_{31}^{2}}{s_{11}^{E}}. \tag{10}$$

σ is the stress along the direction of the rod, ε is the corresponding strain, D is the electric displacement and E the electric field. Concerning the material constants, s_{11}^{E}, d_{31} and ϵ_{33}^{σ} are respectively the elastic compliance at constant electric field, the piezoelectric voltage coefficient and the permittivity at constant stress. Those constants are related to the strain-charge form of the linear piezoelectricity. They are here highlighted because it is the ones that are commonly presented in the material data sheets as for the PIC 151.

At a global level, if the lenght l_p of a piezoelectric element is sufficiently small compared to the studied wavelength, the strain ε can be considered constant and thus defined thanks to a difference between the positions of the left and right ends of the element, U_{p_L} and U_{p_R}. Moreover, for small thickness h_p, E, which is derived from the potential V_p, can also be regarded as a constant. Consequently, the integration of the local piezoelectric formulation of Eq. (10) leads to a system applying to global variables related to the piezoelectric element:

$$\begin{cases} \dfrac{N_p}{S_p} = Y_p^{E}\dfrac{\dot{U}_{p_R} - \dot{U}_{p_L}}{j\omega l_p} + \bar{e}_{31}\dfrac{V_p}{h_p} \\ -\dfrac{i_p}{j\omega A_p} = \bar{e}_{31}\dfrac{\dot{U}_{p_R} - \dot{U}_{p_L}}{j\omega l_p} - \bar{\epsilon}_{33}^{\varepsilon}\dfrac{V_p}{h_p} \end{cases}. \tag{11}$$

If b is the width of the piezoelectric element, $S_p = h_p b$ is its cross section and $A_p = l_p b$ its surface area. $Y_p^{E} = \bar{c}_{11}^{E}$ is the Young modulus of the piezoelectric material that impacts the normal force N_p, which is uniformly distributed on the cross section. The intensity i_p passing through the surface area is defined relatively to the piezoelectric voltage V_p by considering the element as a power source respecting the passive sign convention.

Then, a last step consists in transforming the previous equations into a complete global system, even for the material properties. This can be done by expressing the stiffness of the considered piezoelectric element at constant electric field K_p^{E}, its capacitance at constant strain C_p^{ε} and its global piezoelectric constant e_p:

$$\begin{cases} -N_p = \dfrac{K_p^{E}}{j\omega}(\dot{U}_{p_L} - \dot{U}_{p_R}) + e_p V_p \\ i_p = -e_p(\dot{U}_{p_L} - \dot{U}_{p_R}) + j\omega C_p^{\varepsilon} V_p \end{cases}, \text{ where } \quad K_p^{E} = \frac{Y_p^{E} S_p}{l_p}, \quad e_p = -b\bar{e}_{31} \quad \text{and} \quad C_p^{\varepsilon} = \bar{\epsilon}_{33}^{\varepsilon}\frac{A_p}{h_p} \tag{12}$$

The global formulation given by Eq. (12) can be illustrated through the electric scheme introduced in Figure 8. It is remarkable that this model corresponds exactly to the coupling part of the architecture presented in Figure 7. The mechanical part refers to the left network and the electrical part to the right one. Only the inductors are missing and this is due to the fact that no mass of the piezoelectric material as well as no inductive behavior was taken into account in the global formulation of Eq. (11). Regarding the inductance $\hat{L}$, it is related to the prospective components that can be linked to the piezoelectric element. Concerning L, it is equivalent to the mass of the element and it can be added afterwards if the discretization into a unit cell is performed.

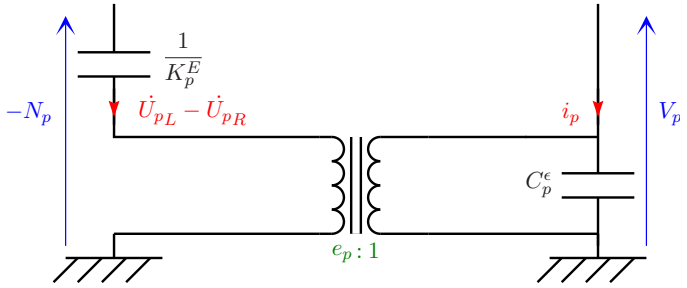

Figure 8: Global model of the piezoelectric element

4.3 Coupling of mechanical and electrical structures

The previous considerations regarding the global model of a piezoelectric element showed that it can take the role of the coupling part in the connection of a mechanical lattice to an electrical network. Each unit cell would be fitted with one piezoelectric element, which will convert the mechanical energy into electric energy and reciprocally. Therefore, all of this can apply to the control of a rod with periodically distributed piezoelectric patches as it was studied by Thorp et al. [8] and then extended for beams [10, 9]. Here, what differs from the previous studies is that the rod, which is a continuous structure, is modeled by a discrete lattice. This together with the electrical representation of the problem considerably simplifies the analysis and the application of the modal coupling to the two structures.

The unit cell of the coupled problem is represented in Figure 9. A main structure consisting of N sections of length a, width b and thickness h_s is symmetrically covered with pairs of piezoelectric patches polarized in opposite directions. Those patches are electrically connected in parallel, their negative electrodes being linked to the ground and the positive electrodes to a network of inductive components. The transformation of this sub-structure into discretized coupled unit cells, as presented electrically in Figure 7, requires to find the global mechanical and electrical properties. About the first ones, a direct observation of the mechanical part of the coupled unit cell leads to the solution:

$$m = \rho_s S_s a + 2\rho_p S_p l_p \quad \text{and} \quad \frac{1}{K} = \frac{1}{K_{sp}} + \frac{2}{K_s} = \frac{l_p}{Y_s S_s + 2Y_p^E S_p} + \frac{a - l_p}{Y_s S_s}, \tag{13}$$

where m is the total mass of the unit cell and K its stiffness, with $S_s = h_s b$. This global stiffness comes from the analysis of three serial spring of stiffness K_s, K_{sp} and K_s, after having considered that all the cross sections remain undeformed.

Finding the global coupling constant e requires to come back to Eq. (12) that apply independently to the each of the two piezoelectric patches placed in the configuration of Figure 9. Thus, the current going to the pair

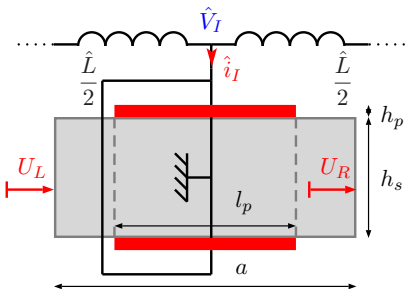

Figure 9: Unit cell of the coupled problem

of patches being $\hat{i}_I = 2i_p$, the problem can be described at the level of the unit cell by

$$\begin{cases} -N_I = \dfrac{K}{j\omega}(\dot{U}_L - \dot{U}_R) + e\hat{V}_I \\ \hat{i}_I = -e(\dot{U}_L - \dot{U}_R) + j\omega\hat{C}\hat{V}_I \end{cases}, \quad \text{where} \quad e = -2b\bar{e}_{31}\frac{K}{K_{sp}}. \tag{14}$$

The force N_I represents the normal force into the unit cell without considering the effect of its mass. It is the equivalent of $-\hat{V}_I$ for the mechanical lattice. One can notice that stiffness takes place in the definition of e. This is due to the fact that the displacements of the ends of the piezoelectric elements, U_{p_L} and U_{p_R}, are not equal to the displacements of the ends of the unit cell, U_L and U_R, because the patches don't cover the entire length a. So, the strain of the patches depends also on the stiffness K and K_{sp}. Indeed, when $\hat{V}_I = 0$, N_I is constant all along the cell and $K(U_L - U_R)$ is equal to $K_{sp}(U_{p_L} - U_{p_R})$.

Concerning the constant defined by $\hat{C}$, it corresponds to the capacitance that would be measured if $U_L - U_R = 0$. Its analytic formulation requires to take into account 3D effects that will not be developed in this study. Nevertheless, it can be emphasize that $\hat{C}$ can be bonded. Its low limit is the capacitance obtained by blocking the patches along the sides of length l_p and b. The high limit is the value obtained when no stress is applied to the ends of the unit cell, which can be measured in a free-free configuration.

Knowing the global properties of the coupled unit cell and that the architecture of the problem is equivalent to the coupling of two lattices of point masses as well as the coupling of two $\hat{L}\hat{C}$ networks, the transfer matrix is obtained from Eq. (8):

$$\begin{pmatrix} \dot{U}_R \\ \hat{i}_R \\ N_R \\ \hat{V}_R \end{pmatrix} = \begin{pmatrix} 1-f & \dfrac{e}{K\hat{C}}\hat{f} & \dfrac{j\omega}{K} & \dfrac{j\omega e}{K} \\ ef_l & 1-\hat{f}\left(1+\dfrac{e^2}{K\hat{C}}\right) & -\dfrac{j\omega e}{K} & -j\omega\left(\dfrac{e^2}{K}+\hat{C}\right) \\ -\dfrac{2K}{j\omega}f\left(1-\dfrac{f}{2}\right) & -\dfrac{e\hat{K}}{j\omega}f\hat{f} & 1-f & -ef \\ \dfrac{e}{j\hat{C}\omega}f\hat{f} & \dfrac{2\hat{f}}{j\hat{C}\omega}\left[1-\dfrac{\hat{f}}{2}\left(1+\dfrac{e^2}{K\hat{C}}\right)\right] & -\dfrac{e\hat{f}}{K\hat{C}} & 1-\hat{f}\left(1+\dfrac{e^2}{K\hat{C}}\right) \end{pmatrix} \begin{pmatrix} \dot{U}_L \\ \hat{i}_L \\ N_L \\ \hat{V}_L \end{pmatrix}, \tag{15}$$

$$\text{where} \quad f = \omega^2\frac{m}{2K} \quad \text{and} \quad \hat{f} = \omega^2\frac{\hat{L}\hat{C}}{2}.$$

As for the previous analysis of purely mechanical coupled lattices, a multimodal tuning can be reached by applying the modal coupling condition

$$\frac{1}{\sqrt{\hat{L}\hat{C}}} = \sqrt{\frac{K}{m}}. \tag{16}$$

From this last equation and the definition of the global constants, it is seen that the inductance to be used for the coupling is proportional to the inverse of the number of unit cells: $\hat{L} \propto 1/N$ for a constant l_p/a ratio. This conclusion, which was highlighted by Maurini et al. [12], induces that the increase of N leads to lower values of $\hat{L}$ and possibly the opportunity to use market components even for the control of low frequencies. Moreover, increasing N enhances the frequency range in which the discretized behavior remains close the continuous one. The electrical network being tuned to the modes of the lattice, it is obvious that it will not completely match the modes of the continuous rod. However, as it was presented previously, above 10 unit cells per wavelength, this difference is acceptable. For example, with 20 cells along a free-free rod, it is possible to influence the 4 first modes of the rod and with $N = 40$ it becomes possible to look until the 8^{th}.

For a study of distributed and independent shunts connected to each of the pairs of piezoelectric patches, the 4×4 matrix presented in Eq. (15) can be condensed in a 2×2 form by setting $\hat{V}_L$ and $\hat{V}_R$ to 0. In this configuration, it is the value of $1/\sqrt{\hat{L}\hat{C}}$ that sets the frequency that will be damped. Thus, $\hat{L} \propto N$ and the inverse of the previous conclusion is expected: large inductance will be needed in the case of a high number of unit cells.

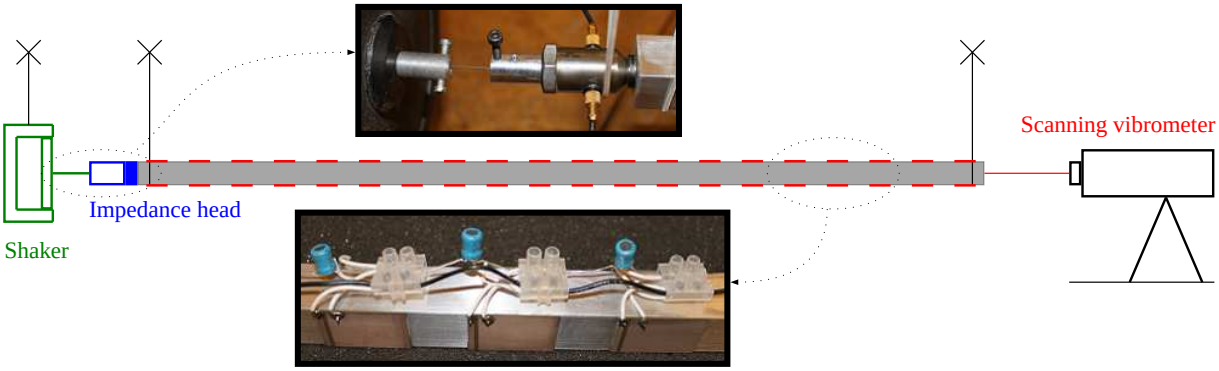

Figure 10: Experimental setup

5 Experimental results

5.1 Experimental setup

The expectations concerning the coupling of mechanical and electrical structures can be verified experimentally. For this purpose a one meter duralumin rod is periodically covered with $N = 20$ pairs of piezoelectric patches. Referring to Figure 9, the geometry of the setup is presented in Table 1.

	Rod (AU4G)	Patches (PIC 151)
Length	$l_s = Na = 20 \times 5$ cm	$l_p = 3$ cm
Width	$b = 2$ cm	$b = 2$ cm
Thickness	$h_s = 2$ cm	$h_p = 0.5$ mm
Density	$\rho_s = 2800$ kg/m^3	$\rho_p = 7800$ kg/m^3
Young modulus	$Y_s = 74$ GPa	$Y_p^E = 1/s_{11}^E = 1/(15\ 10^{-12})$ GPa
Piezoelectric coefficient	-	$d_{31} = -210\ 10^{-12}$ C/N
Permittivity	-	$\epsilon_{33}^\sigma = 2400\epsilon_0 = 2400 \times 8.85\ 10^{-12}$ F/m

Table 1: Geometry and material properties

The selected piezoelectric material is the PIC 151 ceramic from the company Physik Instrumente (PI). It was chosen accordingly to previous studies [5] in order to keep the possibility to extend some of their results. The properties of the PIC 151 are also described in Table 1, which reports values coming from the PI data sheet. The resulting structure is suspended by elastic straps in order to tend to a free-free configuration. Then, as presented in Figure 10, a suspended shaker is connected to one end of the rod through an impedance head that measures the displacement and the transmitted force. At the other end, a scanning laser vibrometer measures the velocity.

During measurement, a white noise excitation is generated and two signals are analyzed: the velocity coming from the vibrometer and the force measured by the impedance head. The last step consists in obtaining the transfer function between the velocity and the force signals. To this end, a fast Fourier transform is performed on a 11.5 kHz frequency range with a resolution set to 4 Hz.

Concerning the electrical components, in a goal of a completely passive damping, inductors are selected in various industrial series as the 09D by Panasonic or the RL622 by Bourns. The inherent resistance of the inductors is presented in their data sheets. This value is not negligible and justify the absence of damping optimization in the previous theoretical study. Indeed, one can see from numerical simulations with a resistor serially added to the inductor, that the optimal value is lower than the practical possibilities when referring to the previous standard series. It is thus not possible to improve the resistance but in the same time, no specific resistors need to be added, which simplifies the network.

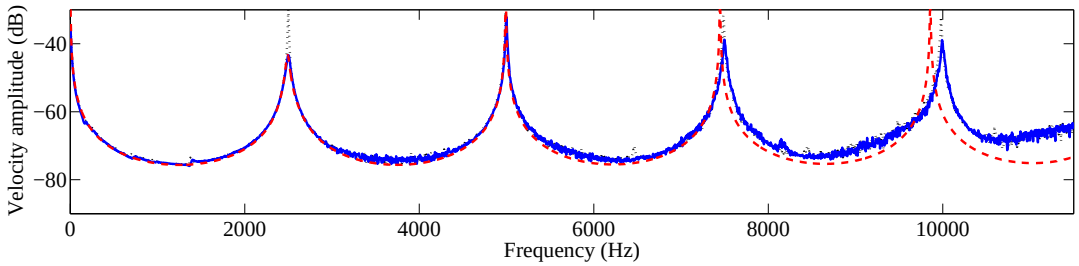

Figure 11: Frequency responses for the distributed shunts strategy - (· · ·) for short circuits, (—) for resonant shunts and (– –) for the discretized model with resonant shunts

The standard inductors having discrete values, it is not always possible to find components that suits with the calculated inductance needed for a modal coupling. This problem appears if $\hat{C}$ is considered equal to the capacitance of the pair of patches. However, it is possible to add real capacitors in parallel to the piezoelectric patches. This increases the capacitance $\hat{C}$ and gives a degree of freedom in the choice of $\hat{L}$. Nano or tenth of nano Farad are available in the Vishay MKT 368 series proposing metallized polyester film capacitors. This suits with the tuning of $\hat{C}$ which was evaluated to 34 nF without adding capacitors.

5.2 Distributed resonant shunts for the damping of longitudinal waves

The first experiment consists in the study of the influence of independent resonant shunts distributed all along the structure. It is chosen to keep also the periodicity of the electrical structure by using identical shunts. If the vibration attenuation of the first mode of the free-free rod is wanted, the natural frequency of the shunts needs to be tuned around 2500 Hz. This value can be approached by selecting a 100 mH Bourns inductor which presents a resistance close to 210 Ω. Then, a correction of the capacitance needs to be performed by adding a 4.7 nF capacitor. Those values are given with $\pm 10\%$, which is a classical tolerance for this kind of components. The inductor and the capacitor are both placed in parallel to each pair of piezoelectric patches, independently on all the unit cells.

The results are presented in Figure 11 where the four first modes of the free-free rod are observed. One can see that the piezoelectric passive damping system gives a reduction of about 15 dB on the velocity amplitude of the 1^{st} mode. On the contrary, the second mode presents no visible attenuation. This agrees with the theoretical study and the frequency response obtained in Figure 3 for a similar strategy. Nevertheless, a non expected reduction of the 3^{rd} and 4^{th} modes is experimentally observable. For now, this effect is not clearly explained but a first assumption would be that it is due to non characterized resistive effects in the added electrical components.

Concerning the theoretical representation, it does not completely suit with the experiments if e is computed from Eq. (14). The reduction of e comes from glue effects and 3D effects that are not taken into account. To correct this influence, e was experimentally calibrated and the obtained value corresponds to 70% of the theoretical one. Another remarkable observation is the shift between the theoretical curve and the experiments when it goes to high frequencies. This can be clearly explained by the fact that the theoretical curve represents the discrete model. As said previously, at the 4^{th} mode is reached the limit of 10 unit cells per wavelength. The validity of the model is obviously not suddenly reduced but the shift applies increasingly and at this frequency it is no more negligible.

5.3 Multimodal network for longitudinal waves

The second experiment is related to the validation of the multimodal damping strategy. For the present geometry and material properties, the application of the modal coupling condition of Eq. (16) gives an inductance $\hat{L}$ around 2.9 mH. This value was not proposed in the considered series but it is possible to

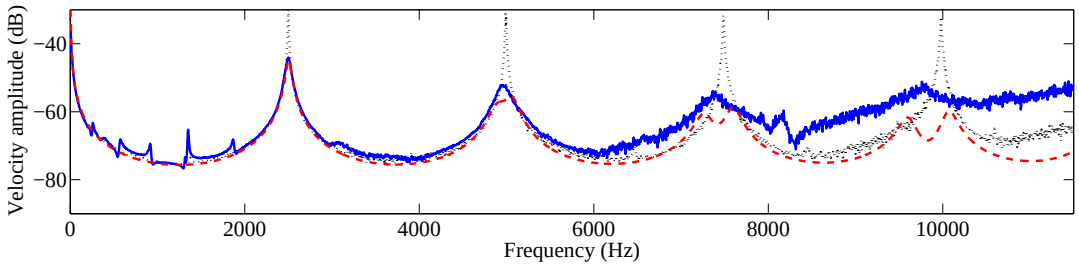

Figure 12: Frequency responses for the multimodal damping strategy - ($\cdots$) for short circuits, (—) for the optimal network and (– –) for the discretized model with the optimal network

find 2.7 mH inductors. Consequently, this induces the adjustment of $\hat{C}$ by adding a capacitor of 2.2 nF. The electrical network was thus realized with those components by linking successive unit cells with the inductors and by placing the capacitors in parallel to the pairs of piezoelectric patches. The ends of the line are closed by a $\hat{L}/2$ inductance obtained by paralleling two of the previous inductors. This allows respecting the zero voltage boundary condition which is the equivalent of the free-free mechanical condition.

The results obtained with the electrical network are illustrated in Figure 12. The performances are significant as the reduction is about 15 dB for the first mode and more than 20 dB for the other ones. This clearly validates the concept of multimodal damping by the use of a passive electrical network. Moreover, the second half of the experimental curve seems to represent a less beneficial situation than the real behavior. The reduction of vibration being strong on all the frequency range, the non predictable noise is no more negligible compared to the primary velocity signal. This enhances the noise level in the representation and disturbs strongly the analysis above 8 kHz.

5.4 Non-optimal network for transverse waves

When looking at damping of transverse waves, it becomes clear that the previous network is not optimal. Indeed, it was defined from a discretization of a structure satisfying the dispersion relation for longitudinal waves. This methodology gives a network with natural frequencies that are close to those of the continuous structure and that are consequently approximately equally spaced in the frequency range. This does not suit with the vibration of a beam, for which the modal density decreases accordingly to the non-linear dispersion relation for transverse waves. In order to find the optimal network for bending, one can follow the same steps than those illustrated in the present analysis. The size of the system of equations is doubled and the obtained electrical analogue is the same as the one presented by Andreaus et al. [13]. Nevertheless, the non-optimal network can be used to damp a particular mode. This requires to adjust the position of the n^{th} mechanical mode to be controlled, on the position of the n^{th} electrical mode of the network. Compared to the distributed shunts strategy, the advantage is that the value of the inductance can be reduced by increasing the number of unit cells.

With the previous 100 mH inductors and 4.7 nF capacitors, it is possible to create a network with the same architecture than the one used for the multimodal damping. The thing is that with those values, the 9^{th} natural frequency of the network is close to the 9^{th} bending frequency. As expected, the experimental results presented in Figure 13 show a strong reduction of the amplitude of the 9^{th} mode. It is also very interesting to notice that the non-optimal network has a non negligible effect on modes for which it was not tuned. For example, the 3^{rd} electric mode is very close to the 5^{th} mechanical mode and induces an important reduction. Likewise, the 10^{th} mechanical mode is just between two close electric modes, which create a large damping. So, this experiment already shows that a non-optimal network can have important multimodal effects on the reduction of transverse vibration.

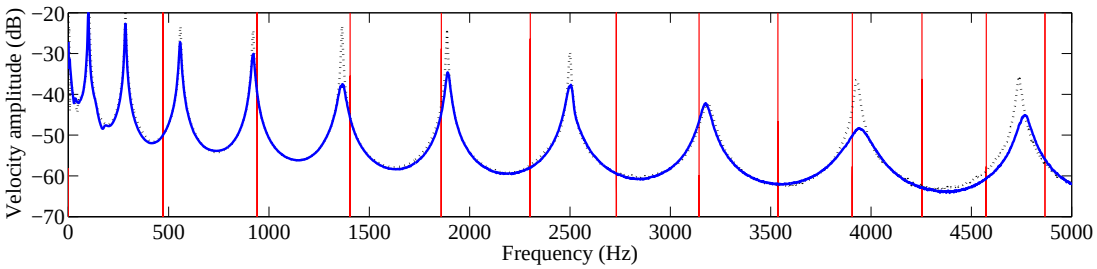

Figure 13: Frequency responses in bending with the non-optimal network - (· · ·) for short circuits, (—) for the non-optimal network and (—) for the position of the electric modes

6 Conclusions

Through a transfer matrix approach, it was seen that a continuous wave-guide can be studied as a periodic structure where the number of unit cells remains free. Then, a rod was modeled by a lattice of point masses that are serially connected with springs representing the stiffness of a section of the structure. The length of this section limits the maximum frequency of the analysis, as a continuous behavior can be approached only if the considered wavelength is large compared to the length of the discretization. Over a second phase, it was looked for a solution that could lead to the conversion of the vibration energy from a finite main lattice to a damping device. A first strategy is to use distributed tuned mass dampers all along the structure by connecting them independently to each of the unit cells. Identical tunings of the natural frequencies lead to the possibility to control only the mode which is placed at this particular position. A second strategy consists in the implementation of a multimodal coupling. This can be obtained by connecting to the main structure its modal equivalent. It requires the equalization of the dispersion relation and the adjustment to similar boundary conditions. Thereby, it is possible to obtain a multimodal tuned mass damping that apply to all the natural frequencies.

In the context of vibration damping by piezoelectric materials, an electromechanical analogy shows that the distributed strategy is equivalent to the use of periodical resonant shunts all along a one-dimensional structure. Moreover, the electrical analogues of a lattice of point masses and a piezoelectric element point out the fact that a multimodal strategy can be achieved by an electrical network linking all the piezoelectric patches. Thanks to a global formulation at the level of the unit cell, a 4×4 transfer matrix is obtained for the study of longitudinal waves. This considerably simplifies the continuous problem and the application of the modal coupling condition. Experiments on a rod validates the efficiency of the method with a completely passive network. The performances are considerable on all the observed modes which validates the efficiency of this damping strategy. Furthermore, the presented network was tested for damping of transverse waves and it appears that multimodal effects are non negligible although the modal coupling is only respected for one mode.

Finally, an efficient discretized model related to the coupling of two structures of different natures was presented for the propagation of longitudinal waves. The experimental analysis was extended to the damping of bending modes and it showed interesting performances that need to be closely analyzed. Another extension is the theoretical study of the diminution of the coupling coefficient, as well as the determination of the capacitance of the glued piezoelectric patches. All of this will be conducted together with the analysis of optimal networks for transverse wave, whose performances seem already very promising.

Acknowledgements

We would like to thank the French Ministry of National Education, Higher Education and Research for providing a three year scholarship for doctoral studies related to the present topic.

References

[1] D.M. Mead, *Wave propagation in continuous periodic structures: research contribution from Southampton, 1964-1995*, Journal of Sound and Vibration, Vol. 190, No. 3, Academic Press (1996), pp. 495-524.

[2] B. R. Mace, D. Duhamel, M. J. Brennan, L. Hinke, *Finite element prediction of wave motion in structural waveguides*, The Journal of the Acoustical Society of America, Vol. 117, No. 5, Acoustical Society of America (2005), pp. 2835-2843.

[3] L. Brillouin, *Wave propagation in periodic structures*, McGraw-Hill (1946).

[4] L. L. Beranek, *Acoustics*, McGraw-Hill (1954).

[5] O. Thomas, J. Ducarne, J-F Deü, *Performance of piezoelectric shunts for vibration reduction*, Smart Materials and Structures, Vol. 21, No. 1, IOPscience (2012), p. 015008.

[6] K. Liu, J. Liu, *The damped dynamic vibration absorbers: revisited and new result*, Journal of Sound and Vibration, Vol. 284, No. 3, Elsevier (2005), pp. 1181-1189.

[7] O. Thomas, J.-F. Deü, J. Ducarne, *Vibrations of an elastic structure with shunted piezoelectric patches: efficient finite element formulation and electromechanical coupling coefficients*, International Journal for Numerical Methods in Engineering, Vol. 80, No. 2, John Wiley & Sons (2009), pp. 235-268.

[8] O. Thorp and M. Ruzzene, A. Baz, *Attenuation and localization of wave propagation in rods with periodic shunted piezoelectric patches*, Smart Materials and Structures, Vol. 10, No. 5, IOPscience (2001), p. 979.

[9] L. Airoldi, M. Ruzzene, *Design of tunable acoustic metamaterials through periodic arrays of resonant shunted piezos*, New Journal of Physics, Vol. 13, No. 11, IOPscience (2011), p. 113010.

[10] B. S. Beck, K. A. Cunefare, M. Collet, *Experimental assessment of negative impedance shunts for vibration suppression on a beam*, Proc. SPIE, Vol. 6928, SPIE (2008), pp. 69281X-69281X-9.

[11] H. Yu, K.W. Wang, J. Zhang, *Piezoelectric networking with enhanced electromechanical coupling for vibration delocalization of mistuned periodic structures - Theory and experiment*, Journal of Sound and Vibration, Vol. 295, No. 1-2, Elsevier (2006), pp. 246-265.

[12] C. Maurini, F. dell'Isola, D. Del Vescovo, *Comparison of piezoelectronic networks acting as distributed vibration absorbers*, Mechanical Systems and Signal Processing, Vol. 18, No. 5, Elsevier (2004), pp. 1243-1271.

[13] U. Andreaus, F. dell'Isola, M. Porfiri, *Piezoelectric passive distributed controllers for beam flexural vibrations*, Journal of Vibration and Control, Vol. 10, No. 5, SAGE Publications (2004), pp. 625-659.

[14] Y. Lu, J. Tang, *Electromechanical tailoring of structure with periodic piezoelectric circuitry*, Journal of Sound and Vibration, Vol. 331, No. 14, Elsevier (2012), pp. 3371-3385.